

# Aerodynamic load characterisation of a low speed aerofoil using particle image velocimetry

B. W. van Oudheusden, E. W. F. Casimiri and F. Scarano

Delft University of Technology  
Delft, The Netherlands

## ABSTRACT

Particle image velocimetry (PIV) measurements of the flow around a wing section are employed as a basis for non-intrusive aerodynamic mean loads characterisation, providing sectional lift, drag and pitching moment. The technique relies upon the application of control-volume approaches in combination with the deduction of the pressure from the PIV experimental data through application of the momentum equation. The treatment can also be applied when the flow is unsteady; in that case time-mean loads are obtained from velocity statistics, through the use of Reynolds-averaged formulation of the governing equations. The procedure was applied in the experimental investigation of a NACA 642A015 aerofoil, in which the PIV approach is validated against standard pressure-based methods (surface pressure distribution and wake rake). The chord Reynolds number considered in the investigation ranges between  $1 - 7 \times 10^5$ . In addition, the consistency and potential performance of the method was assessed by means of synthetic velocity field data obtained from a numerical flow simulation.

## NOMENCLATURE

$c$	chord
$D$	drag
$L$	lift
$M$	pitching moment
$p$	pressure
$u$	velocity
$\alpha$	angle-of-attack
$\rho$	density
$\mu$	dynamic viscosity

## 1.0 INTRODUCTION

The flow around nominally two-dimensional configurations, like aircraft wings or turbine blades, is conveniently studied in cross-sectional planes by means of planar velocimetry techniques, such as particle image velocimetry (PIV) in particular<sup>(1-2)</sup>. PIV has proven to be a convenient and powerful diagnostic tool for wind tunnel flow studies, being capable of delivering instantaneous velocity field data over a complete region of interest, hence revealing and quantifying the instantaneous spatial structures of the flow. When moreover the spatial resolution is sufficient, instantaneous spatial derivatives of the velocity field (hence, vorticity) can be determined as well. This is a significant improvement with respect to probe-based techniques where the flow field information is obtained sequentially, from scanning of the flow field domain. Also, probe-based flow field investigation is inherently intrusive and may be very time-consuming when great spatial detail is required. Several recent development efforts aim at further increasing the capabilities of the PIV technique, notably the extension of its time-resolving and/or three-dimensional capabilities<sup>(3)</sup>, as well as extending its range of applicability to more demanding flow regimes.

In aeronautical design there is a further strong interest for the aerodynamic loads involved in flow-structure interactions, in view of their relevance to aerodynamic performance. In current experimental research practice, the flow field information and the mechanical loads are obtained by separate techniques. Establishing a direct link between flow behaviour and the accompanying fluid loads, by deriving the loads from the flow field information itself, is an appealing approach. Apart from the inherent synchronisation between the different flow aspects, it further removes the necessity of additional and/or intrusive instrumentation of the model itself. An example of such a procedure is the wake-survey method to

determine the drag of an aerofoil<sup>(4,5)</sup>, which is a well-established technique in wind-tunnel operations practice.

The present study reports on the results of using similar flow field approaches for the full force characterisation of an aerofoil section — providing lift, drag and pitching moment — based on the measurement of the flow velocity field around the aerofoil by means of PIV. The feasibility of the approach was confirmed in a preliminary study<sup>(6)</sup>; the present communication reports in detail on the implementation of the procedures and provides more extensive results of the experimental investigation. The chord Reynolds number considered in the investigation ranges between  $1 - 7 \times 10^5$ . In particular, the performance of the different load determination approaches with reducing flow speed will be addressed. The motivation for this is that a velocity-based procedure for loads characterisation may provide an appealing perspective for application in the experimental low-Reynolds number characterisation of aerofoils. Under these conditions the use of standard pressure-based procedures become increasingly unreliable with decreasing dimensions (restrictions on model instrumentation) and flow speeds (reduced dynamic head). For the PIV method, on the other hand, model size and flow speed reductions are readily accommodated without loss of accuracy, by adapting the optical magnification (field of view size) and pulse delay time, respectively.

### 1.1 Principle of operation

The control-volume approach allows to determine the integral load on an object (forces and moments) from an integration of the flow variables over a control volume surrounding this object<sup>(7,8)</sup>, as illustrated in Fig. 1. Several procedures have been proposed recently, that would allow unsteady lift and drag loads to be determined from time-resolved PIV data<sup>(9-14)</sup>, based on variants of the control-volume approach. Required flow field properties are velocity, pressure, density and viscous stresses. Assuming constant density, a direct application of the control-volume formulation requires the velocity and acceleration distribution inside the volume, as well as the pressure on the outer contour. The pressure field is generally not available in a PIV experiment and basically two approaches can be followed to accommodate this. The first is to use a formulation of the control-volume approach from which the pressure has been eliminated<sup>(11)</sup>. The second is to explicitly evaluate the pressure using the momentum equation<sup>(10)</sup>.

Although the above approaches in principle allow to obtain instantaneous pressure and force data, practice seldom permits to perform time-resolved velocity measurements or to determine acceleration with a sufficient level of accuracy. Moreover, in many applications of technical interest it may be sufficient to study the flow in the mean sense, and to provide knowledge of time-mean loads. For this purpose, Reynolds-averaging of the governing equations allows the aerodynamic force and moment on the object to be written in terms of integrals over the contour  $S$  of the control volume:

$$\mathbf{F} = \iint_S (\hat{\boldsymbol{\sigma}} - p\mathbf{I} - \rho \mathbf{u}\mathbf{u}) \cdot \mathbf{n} \, dS \quad \dots (1)$$

$$\mathbf{M} = \iint_S ((\hat{\boldsymbol{\sigma}} - p\mathbf{I} - \rho \mathbf{u}\mathbf{u}) \cdot \mathbf{n}) \times \mathbf{x} \, dS$$

Here,  $\mathbf{u}$  is velocity,  $p$  pressure,  $\rho$  density and  $\boldsymbol{\tau}$  the stress tensor comprising viscous and turbulent contributions:

$$\tau_{ij} = \mu \left( \frac{\partial u_i}{\partial x_j} + \frac{\partial u_j}{\partial x_i} \right) - \rho \overline{u_i' u_j'} \quad \dots (2)$$

where  $\mu$  is the viscosity. Apart from the turbulence terms, all variables are to be interpreted in their Reynolds-averaged ('mean') values, hence, overbars on individual variables have been omitted for notation simplicity. In most aeronautical applications the direct contribution of the viscous stresses can generally be neglected when the control volume's outer contour is taken sufficiently far from the

body, but it may be included for completeness. With density and viscosity constant, the only required flow property not directly measured is the pressure, which is obtained from integration of the momentum equation:

$$-\frac{\partial p}{\partial x_i} = \rho u_j \frac{\partial u_i}{\partial x_j} + \rho \frac{\partial \overline{u_i' u_j'}}{\partial x_j} - \mu \frac{\partial^2 u_i}{\partial x_j \partial x_j} \quad \dots (3)$$

This analysis shows how, under incompressible two-dimensional flow conditions, time-averaged loads can be inferred when planar velocity statistics, such as provided by standard two-component PIV, are available in a surrounding of the wing cross section. Although not required for the conditions of the present application, it has been shown<sup>(15)</sup> that the procedure can be extended to compressible flow conditions, which is relevant for many aeronautical applications at high speed.

## 2.0 LOADS CHARACTERISATION OF A LOW-SPEED AEROFOIL

### 2.1 Objective and methodology

The motivation for the experimental test campaign considered in the present study is to assess the potential of the PIV-based approach for the aerodynamic load characterisation of a low-speed aerofoil section under realistic wind tunnel conditions. For this kind of tests standard procedures based on pressure measurements are available and regularly applied at the laboratory. For this the wing model is equipped with pressure taps to determine the surface pressure distribution, from which the lift and pitching moment are inferred through integration. The drag is determined separately using a pitot-tube wake rake at some distance behind the aerofoil, as described by Jones<sup>(4)</sup>.

The objective of the present study is to validate the PIV-based approach against the standard procedure and investigate its potential for low-Reynolds number testing. For the control-volume based procedure the flow in a complete surrounding of a wing cross section is imaged using planar two-component PIV, which upon image analysis and subsequent statistical processing provides spatial distributions of mean velocity and turbulence terms. The pressure can then be computed from integration of the momentum equation, as discussed above. In the particular application under consideration where a large region of the flow is irrotational, the pressure gradient integration can be restricted to the wake region, while Bernoulli's relation can be applied outside of it. The wake is identified in the measurements based on a threshold value of the vorticity. Further, two different strategies for the pressure integration have been investigated, *viz* integrating the pressure gradient only along the contour of the control-volume used in the load determination (1D integration), or integrating the pressure in the complete wake domain, from which the pressure on the contour is extracted afterwards (2D integration). Although computationally more elaborate, the latter method can be expected to be more robust as it suffers less from local measurement inaccuracy.

Finally, in addition to the contour-volume approach to determine lift, drag and pitching moment, also classical wake-traverse procedures have been applied to derive the drag from the PIV velocity data. In conventional practice the wake traverse has the evident benefit that only flow data (pressure and total pressure) need to be collected in a limited domain of the flow, being the wake region downstream of the wing. However, even with flow field information available in a complete surrounding, the wake approach is likely to prove favourable in obtaining drag. The major reason for the better performance of the wake approach is that it implicitly ensures mass preservation. Any error in mass conservation over the contour will introduce a momentum error in the contour integration, which affects the loads determination, with largest impact on the drag (see

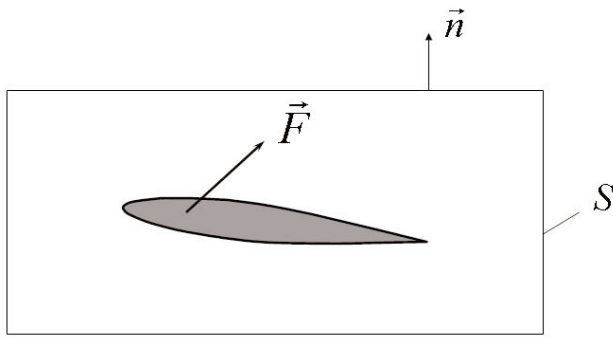


Figure 1. Sketch of the basic working principle.

also the section on the numerical validation). In addition, the wake approach does not suffer from a possible incorrect projection of the total force on the coordinate axes, in case of a slight misalignment of the image orientation with respect to the flow axes.

The expression for the wake-traverse is obtained from the general control-volume formulation, by expanding the contour such that over front, top and bottom surfaces (see Fig. 1) free stream conditions apply. Further invoking integral mass conservation then limits the contour integration to only the rear surface that cuts through the wake<sup>(5)</sup>:

$$D = \int_{wake} (\rho u (U_\infty - u) - (p - p_\infty) - \rho \overline{u'^2}) dy \quad \dots (4)$$

From this expression the classic relation due to Jones<sup>(4)</sup> is obtained by relating the flow in the actual wake analysis plane to a fictitious position far downstream where the pressure has attained its free stream value, assuming that the total pressure  $p_t$  remains constant along the streamline and neglecting turbulent terms:

$$D = \int_{wake} \rho U_\infty u (1 - \sqrt{c_{pt}}) dy \quad \dots (5)$$

This expression is commonly accepted as being valid even close to the trailing edge. It may be further remarked that the location of the drag traverse in the PIV approach is much closer to the aerofoil trailing edge ( $0.5c$  at maximum) than usually permitted for a wake rake (typically 2-3 chord lengths), in view of its possible intrusive effect on the flow. In the present investigation both of the above expressions have been applied, in combination with either the 1D and 2D pressure integration approach. As a general conclusion, it was found that all procedures provided reliable and accurate drag estimates, with the best results (lowest uncertainty, in particular) for the Jones formulation in combination with the 2D pressure integration. For that reason, in the analysis of the experiments only the results for that procedure will be given when considering the wake approach.

With regard to the relevance of the turbulence terms, the theoretical study described in the next section (for attached flow conditions) shows that these are only appreciable in the wake and that they have only a noticeable effect on the drag. Apart from the direct effect of the turbulent momentum fluxes, see Equations 1-2, the turbulence terms also have an influence through the pressure term, see Equation 3. Using the wake drag formulation of Van Dam, Equation 4, and estimating the effect on the pressure in the wake from Equation 3, the complete effect can be assessed approximately as follows:

$$D = \int_{wake} (\rho u (U_\infty - u) - (p_{lam} - \rho \overline{v'^2} - p_\infty) - \rho \overline{u'^2}) dy \quad \dots (6)$$

where  $p_{lam}$  indicates the 'laminar pressure', computed without taking the turbulence term into account. Hence, the dominating turbulence terms are found to be the two normal stresses  $\overline{u'^2}$  and  $\overline{v'^2}$ , which are seen to have counteracting effects:  $\overline{u'^2}$  tends to decrease the drag, while  $\overline{v'^2}$  tends to increase it.

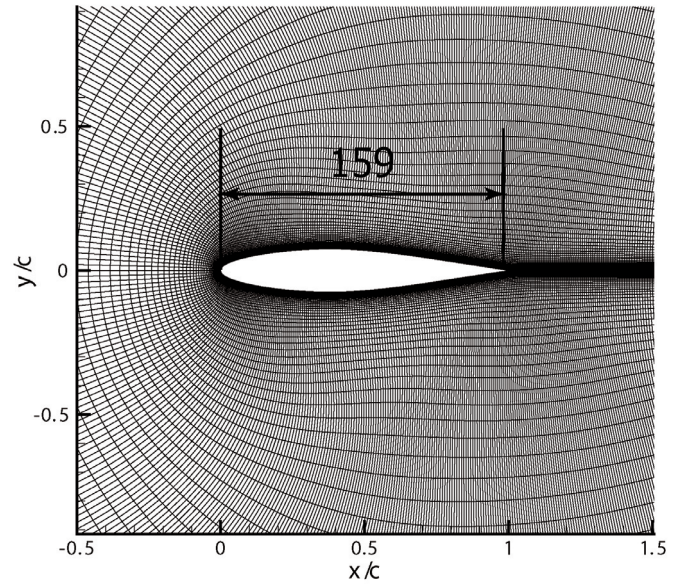


Figure 2. Course grid geometry used in the computational study.

## 2.2 Numerical validation based on synthetic data

Flow experiments were simulated with synthetic velocity field data obtained from a numerical flow simulation, to check the PIV-based procedure for consistency and to assess the potential performance with respect to critical experimental parameters (spatial resolution, measurement uncertainty). The computation was carried out with the commercial CFD code Fluent, and considers the aerofoil used in the experimental investigation (NACA 642A015). For computational convenience a fully turbulent boundary layer is assumed. In the experiment transition is not fixed, however, so the actual drag is likely to be lower than that in the numerical simulation. The flow solver was used with an incompressible two-dimensional steady state model and  $k-\epsilon$  turbulence model and enhanced wall treatment was applied for better modelling near the wall. Three computational grids with increasing resolution were used to verify grid size convergence of the solution. The grids are of C-type layout, as illustrated in Fig. 2 which depicts the mesh in the surrounding of the aerofoil for the coarsest grid. The complete grid extends to 15 chord length upstream of the aerofoil and 25 chord lengths downstream of it. The coarse grid mesh contains 159 cells on each side of the aerofoil, 94 cells normal to the surface and 319 cells behind the aerofoil, giving a total number of cells of approximately 88k. The other meshes were generated by subsequently refining this initial mesh by a factor of 2, giving grids with 355k and 1,422k cells, respectively. Between the intermediate and the finest grid the results for the lift and drag differed by only 0.6%. The solution obtained on the finest mesh was used as data base for the subsequent analysis, comparing the loads provided by numerical integration of the surface forces with those obtained from a contour integral (the 'PIV approach'). For the latter, synthetic PIV data were then subjected to the pressure integration and loads determination procedure, after having extracted the data on a rectangular contour around the wing, centered around the datum chord line. The uncertainty in the load data was estimated by varying the distance of the integration contour to the aerofoil, between 0.25 and 0.5 chord lengths. The nominal interpolation grid has a resolution of 0.6% of the chord, which is similar to the expected PIV experimental conditions. The mesh size of the computational grid is about a factor 5 finer than the interpolation grid. At this interpolation resolution the

**Table 1**  
Results of the synthetic experiment

(a) overall comparison of force determination

AoA	Surface force integration			Contour integral ('PIV approach')		
	$c_l$	$1,000*c_d$	$1,000*c_{m0.25c}$	$c_l$	$1,000*c_d$	$1,000*c_{m0.25c}$
0 deg	0.000	16.38	0.00	0.000±0.000	16.35±0.03	0.00±0.00
5 deg	0.488	25.02	-5.20	0.487±0.000	24.92±0.01	-5.76±0.13

(b) comparison of drag determination procedures

AoA	Surface integration	Contour integral	Wake approach			
			Van Dam (1D)	Van Dam (2D)	Jones (1D)	Jones (2D)
0 deg	16.38	16.35±0.03	16.25±0.05	16.30±0.04	16.41±0.01	16.45±0.00
5 deg	25.02	24.92±0.01	25.24±0.27	25.84±0.03	25.11±0.24	24.88±0.02

**Table 2**  
Breakdown of contour integral computations ( $\alpha = 5^\circ$ )

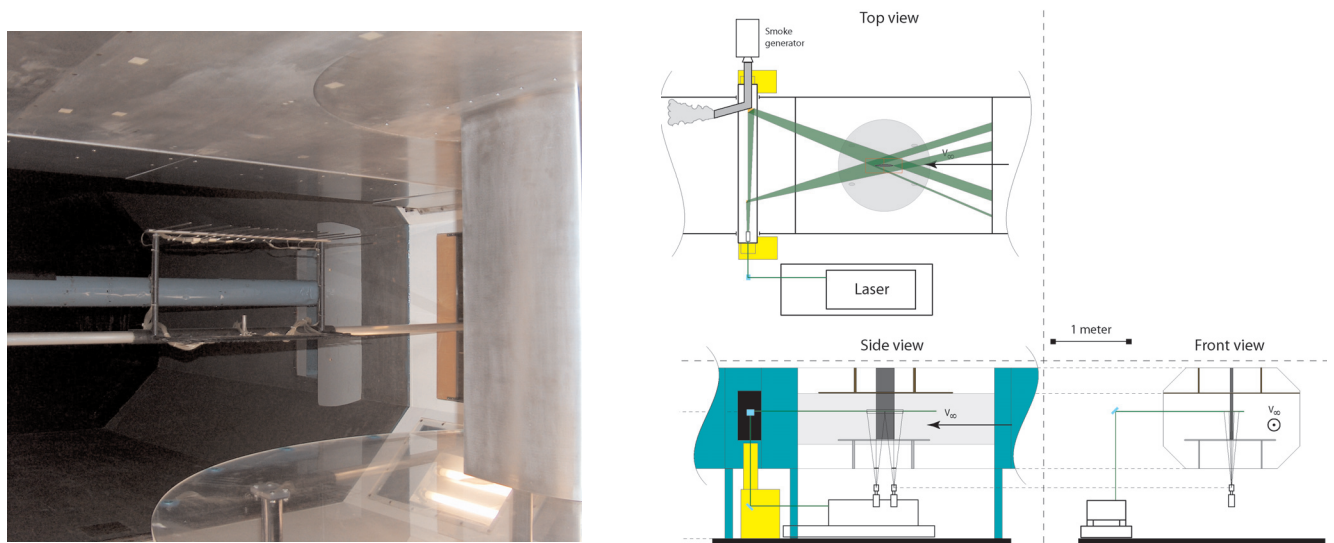
	Wide contour: 1.96c wide × 0.96c high					Narrow contour: 1.44c wide × 0.44c high				
	front	top	rear	bottom	Total	front	top	rear	bottom	Total
<b>Lift</b>										
mean momentum	0.19	-0.02	0.12	0	0.29	0.15	-0.07	0.07	0.01	0.17
pressure	0	0.50	0	0.20	0.71	0	0.68	0	0.15	0.83
turbulent stress	0	0	0	0	0	0	0	0	0	0
total	0.19	0.48	0.12	0.20	1.00	0.15	0.61	0.07	0.16	1.00
<b>Drag</b>										
mean momentum	70.99	1.16	-70.26	-1.58	0.31	29.49	2.07	-29.13	-2.29	0.12
pressure	1.48	0	-0.75	0	0.73	1.76	0	-0.83	0	0.92
turbulent stress	0	0	-0.04	0	-0.04	0	0	-0.04	0	-0.04
total	72.47	1.16	-71.06	-1.58	1.00	31.23	2.07	-30.01	-2.29	1.00
<b>Pitching moment</b>										
mean momentum	16.36	3.07	-15.44	3.61	7.61	8.05	3.18	-7.80	2.51	5.94
pressure	-1.93	-5.18	0.76	-0.26	-6.60	-0.67	-5.52	0.18	1.08	-4.92
turbulent stress	0	0	-0.01	0	-0.01	0	0	-0.01	0	-0.01
total	14.43	-2.11	-14.68	3.36	1.00	7.38	-2.34	-7.63	3.59	1.00

wake is resolved by at least 20 points (conditions apply for  $\alpha = 0^\circ$  where the wake is thinnest). The effect of the spatial resolution of the velocity data was investigated by applying interpolation grids either finer or coarser by a factor 2. The corresponding changes in the load results were less than 0.1% for lift and drag, and 1% for the pitching moment.

Results for the force and moment coefficients are given in Table 1 for angles-of-attack  $\alpha = 0$  and  $5^\circ$  and a chord Reynolds number of 300,000. The typical order of the error observed is  $0.1 \cdot 10^{-3}$  in  $c_d$  (corresponding to 0.5% in drag) and 0.001 in  $c_l$  and  $c_{m0.25c}$ . Note that the value of the moment coefficient is very small, due to the absence of aerofoil camber. The second part of Table 1 contains a comparative assessment of the different drag determination procedures, including the four different wake approaches (Van Dam and Jones refer to the use of Equations 4 and 5 respectively, 1D and 2D indicate the pressure integration method). The conclusion is that in general the Jones method in combination with the 2D pressure integration gives the best results (smallest error and smallest uncertainty), but all methods agree within one percent.

Further insight in the contour-integration procedures is provided by the data given in Table 2, which documents the breakdown of the contour integrals for lift, drag and pitching moment in the different load components (mean momentum, pressure and turbulent stresses)

and the separate segments of the integration contour (front, top, rear and bottom). The values for the individual contributions are expressed relative to the final integral value. Results are given for two sizes of the integration contour around the wing, a narrow contour (1.44c wide × 0.44c high) and a wide contour (1.96c wide × 0.96c high); the latter is comparable in size to the complete field of view in the experimental investigation (1.90c wide × 0.76c high). Looking at the contribution of the different load components to the total contour integral, it is seen that for both lift and drag the contribution of the pressure term is larger than the momentum term, and more so when the contour is closer to the wing. For the pitching moment, the two components are of similar order, but opposite in sign. The turbulent term contributes very slightly (4%) to the drag, while its effect on lift and moment is negligible. A further breakdown of the contour integration to the contributions of the different contour segments further shows that in the lift computation these terms are of similar order. The drag computation, in contrast, involves the difference of large terms, notably the small difference between the inflow and outflow of streamwise momentum. This explains that when assuming that measurement error would introduce similar relative errors on all terms involved, the net effect on drag can be 1-2 orders of magnitude larger than for the lift.



(a) Installation of wing model and wake rake.

(b) PIV experimental arrangement: illumination and viewing geometry.

Figure 3. Experimental wind tunnel arrangement.

### 2.3 Experimental procedure

The experiments were performed in the low-speed low-turbulence wind tunnel of the Aerospace Engineering Department, which is a closed-circuit facility with a test section of  $1.80\text{m} \times 1.25\text{m}$  (width  $\times$  height). The tests were carried out on a wing model with aerofoil section NACA 642A015, with span of  $0.64\text{m}$  and chord of  $0.24\text{m}$ . The wing was suspended vertically from the upper tunnel wall and equipped at its lower free end with a transparent end plate, which allowed optical access to the flow around the wing from a window in the bottom wall of the test section (see Fig. 3). Tests were carried out for a range of incidence angles ( $0$ - $16^\circ$ ) and with free stream velocity between  $6.3$  and  $44.1\text{ms}^{-1}$  (Reynolds number based on chord varies from  $100,000$  to  $700,000$ ).

For each configuration force data were determined with the PIV-based technique and with the standard pressure-based procedures (see above) as means of validation. The pressure distribution was measured with 48 pressure taps along the model contour, from which lift and moment were determined by integration. The wake measurement for obtaining the drag was performed with a rake of total and static pressure tubes (see Fig. 3(a)). The static pressures were measured at 16 points and the total pressure at 67 points. The minimum interval spacing between the tubes applied in the central part of the wake is  $24\text{mm}$  for the static pressure and  $3\text{mm}$  for the total pressure. With the total wake rake width being ca.  $500\text{mm}$ , this assured that under all conditions considered the entire wake was captured, with sufficient resolution of at least 15-20 points to describe the total pressure defect in the wake. Pressures are measured with a liquid-column multi-tube manometer; the liquid level is electronically read with fibre-optical cells with an accuracy of  $0.1\text{mm}$  liquid column (corresponding pressure accuracy is  $1\text{Pa}$ ). For the velocity range where the pressure resolution is not the limiting factor (above  $20\text{ms}^{-1}$ ) the overall uncertainty in the force coefficients is estimated at  $0.005$  for lift and  $0.001$  for drag.

The experimental configuration for the PIV experiments is further detailed in the views of Fig. 3(b). The flow seeding consists of

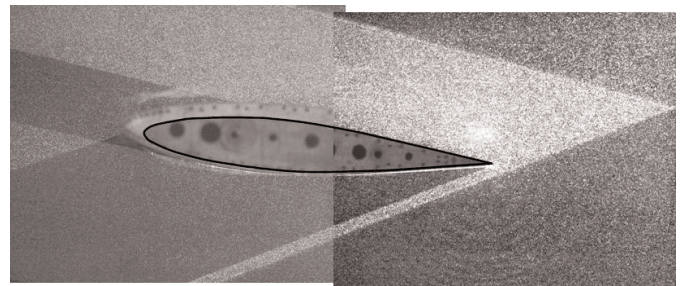


Figure 4. Composite particle image from the two cameras.

$1.5\mu\text{m}$  droplets generated by a fog machine and introduced just downstream of the test section. This ensured minimum intrusiveness of the seeding inlet and provided a proper distribution into the flow when returning to the test section after recirculation of the wind tunnel conduct. The illumination source is a Spectra-Physics Quanta-Ray PIV 400 pulse Nd:YAG laser with a wavelength of  $532\text{nm}$  and energy of  $400\text{mJ/pulse}$ . The laser sheet thickness was about  $3\text{mm}$ . Two CCD camera's ( $1,280 \times 1,024$  pixel and  $1,376 \times 1,040$  pixel, respectively) with  $35\text{mm}$  objectives were used in a side-by-side configuration to produce a composite elongated view around the wing cross section, measuring  $1.90 \times 0.76$  chord lengths ( $455\text{mm} \times 182\text{mm}$ ), extending from  $0.38c$  upstream of the leading edge to  $0.52c$  downstream of the trailing edge. In order to be able to apply the control volume approach the illumination of the wing surrounding is necessary, for which the expanded laser sheet was introduced downstream of the test section and projected onto the model from two mirrors placed on opposite sides of the tunnel (see Fig.3 (b)). The pulse separation was chosen such that the free stream velocity produced a particle displacement of about 7 to 10 pixels. To illustrate the illumination and viewing procedure, a composition picture of a sample particle image provided by the two cameras is shown in Fig. 4, with the position of the wing cross section in the illumination plane overlaid. Some regions above the aerofoil in the view of the

upstream camera) are observed where the flow is shielded by the viewing perspective, hence, no velocity data can be obtained here. These regions will be masked in the subsequent data presentation. Also visible is that, although the split-projection approach allows a complete surrounding of the wing cross section to be illuminated, regions of significant different illumination strength are present. To avoid that the sharp interfaces that result from the laser beam edges and the model shadow would have a dominating effect in the image cross correlation, the particle images were normalised with the local mean (ensemble-averaged) intensity.

Image analysis was carried out with a window-deformation and iterative multi-grid cross-correlation algorithm (LaVision Davis 7.0),

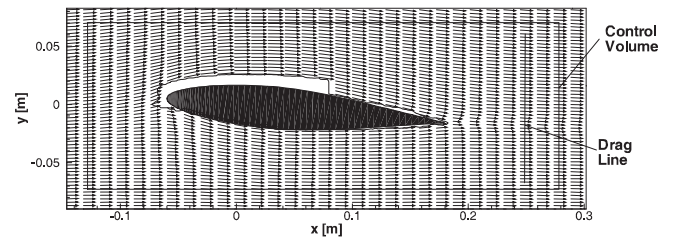


Figure 5. Mean velocity field and the integration contours ( $U_\infty = 19 \text{ ms}^{-1}$ ,  $Re = 300,000$ ).

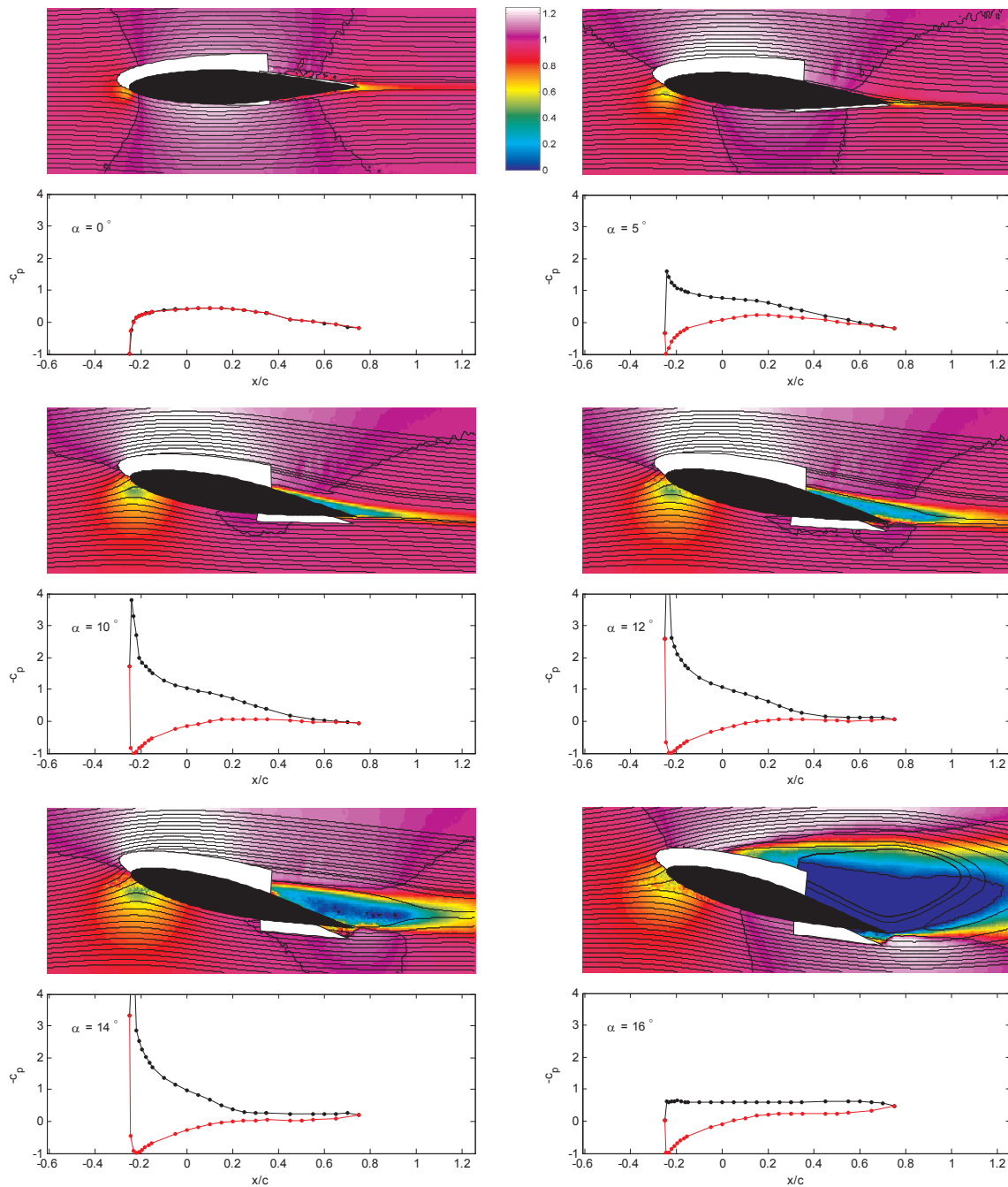


Figure 6. Experimental airfoil characterisation for  $Re = 700,000$ : flow field from PIV (colour contours depict streamwise component  $u/U_\infty$ ) and surface pressure distribution (black: top surface, red: lower surface).

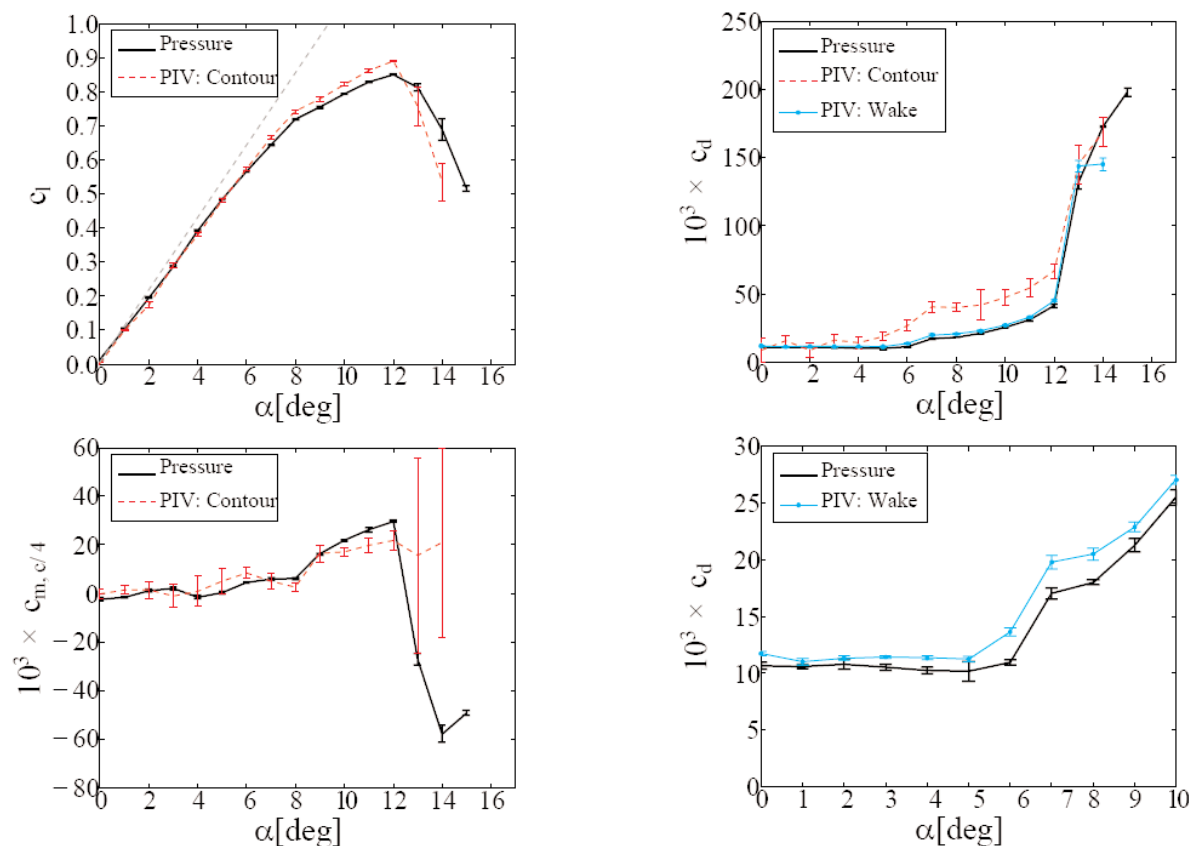


Figure 7. Comparison of load determination with PIV or pressure measurements ( $Re = 300,000$ ).

using an interrogation window size of  $32 \times 32$  pixels and an overlap factor of 75%, yielding a measurement grid with spacing of ca. 1.45 mm (0.6% chord). For each configuration a data ensemble size of ca. 100 image pairs was obtained at an acquisition rate of 2.0Hz. The uncertainty on the averaged velocities is about 0.1% of the free stream velocity in laminar flow regions and approximately 1% in turbulent flow regions. The measurement accuracy of the mean velocity by PIV is primarily dominated by the cross-correlation accuracy (for individual vectors) and by the convergence uncertainty in the procedure of averaging the data ensemble. For fairly uniform velocity regions, advanced cross-correlation algorithms are considered to be accurate by at least 0.1 pixel displacement, yielding an accuracy of at least 1% of  $U_\infty$  on individual vectors. For steady flow the convergence error in the mean is then approximately 0.1% of  $U_\infty$ , given the ensemble size of 100. In the wake, where the effect of turbulent velocity fluctuations on the mean value convergence exceeds that of the effect of the single vector accuracy, the convergence error is estimated to be about 1% of  $U_\infty$  (given 10% velocity fluctuations and ensemble size of 100). The velocity bias error due to the optical distortion as a result of the short focal length of the lenses is maximum ca. 0.4% of the free stream velocity, as estimated from velocity measurements in the empty test section. An example of the field of view and a typical mean velocity field is displayed in Fig. 5, for a free stream velocity of  $19\text{ms}^{-1}$  ( $Re = 300,000$ ), where the velocity vector field has been depicted strongly downsampled for clarity of presentation. As described previously, the bands near the aerofoil are the flow regions masked by the viewing perspective.

For all the experiments the same procedure is applied to determine the free stream conditions. The free stream velocity in the test section is obtained from a calibration of the empty test section, in relation to a reference pressure difference over the wind tunnel contraction, at a sufficient distance upstream of the test section. Free stream density and pressure are computed from the tunnel air temperature measured in the settling chamber, and the ambient atmospheric pressure. As the main objective in the present investigation is the comparative assessment between the two procedures (pressure-based and PIV-based), no wind tunnel corrections have been applied to the force data.

### 3.0 RESULTS

Wind tunnel experiments were carried out for the aerodynamic characterisation of the aerofoil, varying the incidence angle in increments of  $1^\circ$ , for a free stream velocity of  $18.8\text{ms}^{-1}$  ( $Re = 300,000$ ) and  $44.1\text{ms}^{-1}$  ( $Re = 700,000$ ). In addition, to investigate the Reynolds number influence as well as to assess the impact of flow velocity magnitude on the accuracy of the load determination, the flow velocity was varied stepwise between 6.3 and  $44.1\text{ms}^{-1}$  ( $Re = 100,000$  to  $700,000$  with increments of 100,000), for two angles of attack, *viz*  $\alpha = 0^\circ$  and  $5^\circ$ . Figure 6 provides a synthesis of the flow characterisation for  $Re = 700,000$ , showing for a selected number of incidence angles the flow field structure as obtained with PIV (streamlines and velocity colour contours) together with the surface pressure distribution. As reflected by both the streamline patterns

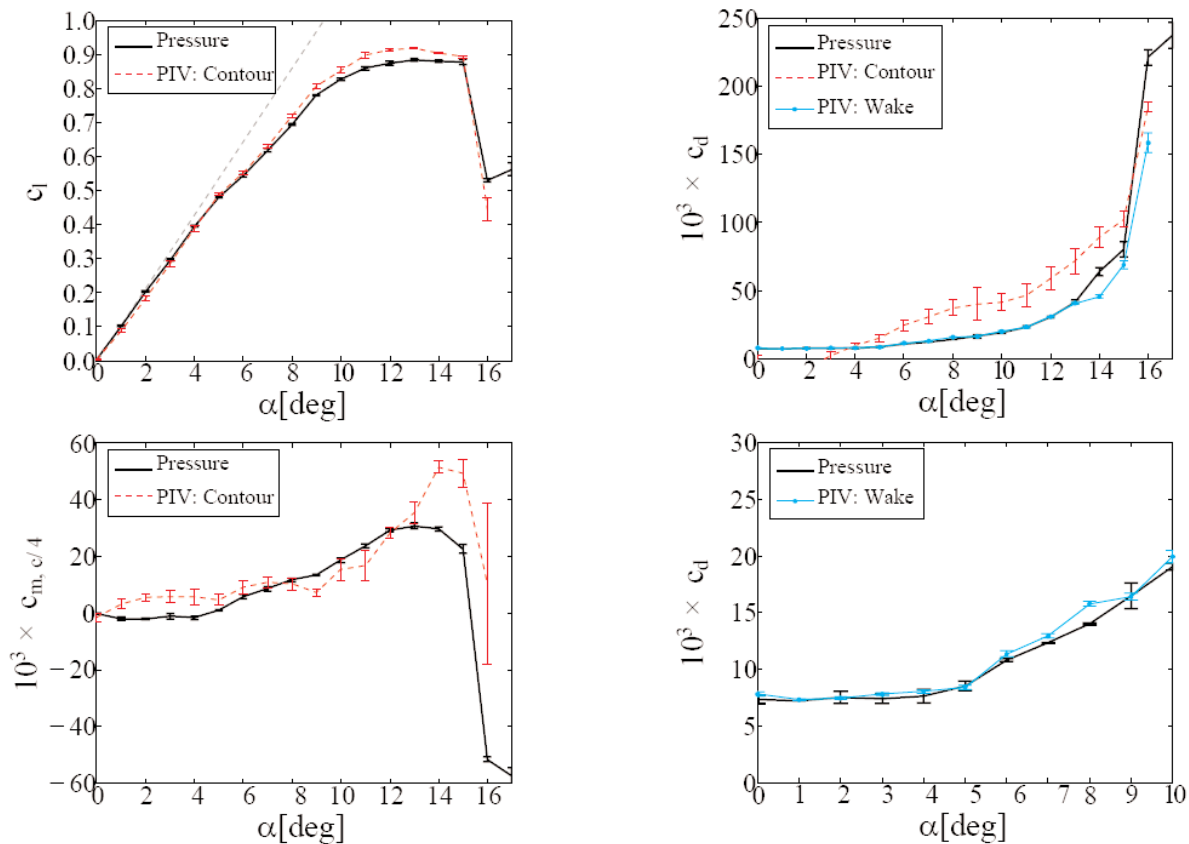


Figure 8. Comparison of load determination with PIV or pressure measurements ( $Re = 700,000$ ).

and the pressure distributions, trailing edge stall sets in near  $\alpha = 10^\circ$ , while the aerofoil has entered deep stall at  $\alpha = 16^\circ$ .

The lift, drag and moment coefficients were computed from the PIV velocity fields by means of the control volume method, taking a contour around the aerofoil as illustrated in Fig. 5. An uncertainty estimate of the coefficients values was based on the different results obtained by changing the size of the contour, in which the distance to the cross section was varied between 0.35 and 0.5 chord lengths (in 25 steps). Because of the low value of the drag, application of the contour procedure yielded unacceptably large relative errors for this parameter, and the drag-determination procedure is much improved by introducing a classical wake approach instead. Varying the location of the wake traverse, between 0.25c and 0.5c behind the trailing edge, again provided an estimate of the drag uncertainty.

Results for the lift, drag and moment as function of incidence are given in Fig. 7 for  $Re = 300,000$  and in Fig. 8 for  $Re = 700,000$ . The error bars (corresponding to  $\pm$  two rms deviations) indicate the uncertainty range of the data. For the incidence range up to maximum lift, average uncertainty (i.e. variability, in the rms sense) on the coefficients for the PIV-based method are 0.003 for the lift and  $1.5 \times 10^{-3}$  for the pitching moment, while for the drag this is  $3 \times 10^{-3}$  for the contour approach and  $0.3 \times 10^{-3}$  for the wake approach. Mean differences between PIV and pressure based data, for the flow conditions considered, depend on the incidence range of interest. At  $Re = 300,000$  and for small incidence, inside the laminar bucket, the

mean differences are 0.012 for the lift coefficient,  $0.9 \times 10^{-3}$  for the drag coefficient using the wake approach ( $5.3 \times 10^{-3}$  with the contour approach) and  $3 \times 10^{-3}$  for the moment coefficient. For larger incidence, the mean differences increase, especially for the aerofoil in stall. This is likely to be related to the increased degree of unsteadiness of the flow which results in poorer convergence of the mean velocity data. The mean differences between PIV and pressure data for  $Re = 700,000$  are assessed at 0.011 for the lift coefficient,  $0.3 \times 10^{-3}$  for the drag coefficient using the wake approach,  $9.5 \times 10^{-3}$  for the drag obtained by the contour approach and  $6 \times 10^{-3}$  for the pitching moment coefficient (considering only the laminar bucket,  $\alpha < 5^\circ$ ). For both Reynolds numbers the drag coefficient based upon the wake-survey approach has good agreement with the pressure data.

As mentioned before the standard pressure measurement becomes increasingly inaccurate for decreasing flow velocity, as is reflected in Fig. 9 which displays the variation of lift and drag coefficients with flow velocity (expressed in terms of the Reynolds number). The accuracy of PIV in principle remains independent of the flow velocity magnitude, and therefore the accuracy of the load determination is largely unaffected by a decrease in flow velocity; this is especially evident for the results of the drag coefficient. This property makes the PIV based load determination an appealing technique for experimental low-Reynolds number aerofoil characterisation.

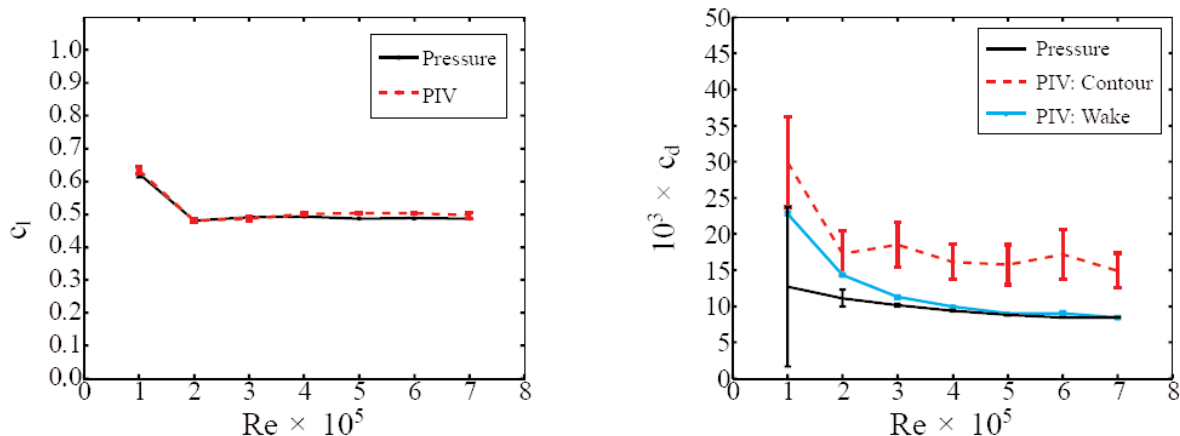


Figure 9. Effect of Reynolds number on load determination with PIV or pressure measurements ( $\alpha = 5^\circ$ ).

## 4.0 CONCLUSIONS

The approach to determine integral loads from planar velocimetry data obtained with PIV was considered as a means for non-intrusive aerodynamic load characterisation of a low-speed airfoil. Lift, drag and pitching moment can be obtained from contour integrals of the velocity data, with the pressure being determined from integration of the momentum equation. Synthetic data obtained from CFD were used to assess the validity of the approach. In the experimental phase of the investigation, PIV results were validated with those obtained from pressure measurements (surface pressure distribution and wake rake). With the flow being predominantly steady, it was found that an ensemble size of 100 turned out to be sufficient to produce force data with acceptable accuracy (estimated velocity uncertainty of 0.1% of the free stream velocity). The lift and pitching moment were determined with the contour approach, while for the drag a wake-survey approach was found to improve accuracy significantly. The typical overall uncertainty of load components (including variability as well as bias with respect to the pressure data) that could be achieved in the present investigation are 0.01 for the lift coefficient,  $1 \times 10^{-3}$  for the drag coefficient and  $4 \times 10^{-3}$  for the moment coefficient.

## REFERENCES

- ADRIAN, R.J. Particle imaging techniques for experimental fluid mechanics, *Ann Review of Fluid Mech*, 1991, **22**, pp 261-304.
- RAFFEL, M., WILLERT, C.E. and KOMPENHANS, J. *Particle Image Velocimetry*, 1998, Springer-Verlag, Berlin.
- ADRIAN, R.J. Twenty years of particle image velocimetry, *Experiments in Fluids*, 2005, **39**, pp 159-169.
- JONES, B.M. Measurement of profile drag by the Pitot-Traversal method, ARC R&M No 1688, January 1936.
- VAN DAM, C.P. Recent experience with different methods of drag prediction, *Prog in Aerospace Sci*, 1999, **35**, pp.751-798.
- VAN OUDHEUSDEN, B.W., SCARANO, F. and CASIMIRI, E.W.F. Non-intrusive load characterization of an airfoil with PIV, *Experiments in Fluids*, 2006, **40**, pp 988-992.
- ANDERSON, J.D. *Fundamentals of Aerodynamics*, Second edition. McGraw-Hill, New York.
- BATCHELOR, G.K. *An Introduction to Fluid Dynamics*, 1991, Cambridge University Press, Cambridge, 1967.
- LIN, J.C. and ROCKWELL, D. Force identification by vorticity fields: techniques based on flow imaging, *J Fluids and Structures*, 1996, **10**, pp 663-668.
- UNAL, M.F., LIN, J.C. and ROCKWELL, D. Force prediction by PIV imaging: a momentum based approach, *J Fluids and Structures*, 1997, **11**, pp 965-971.
- NOCA F., SHIELDS, D. and JEON, D. A comparison of methods for evaluating time-dependent fluid dynamic forces on bodies, using only velocity fields and their derivatives, *J Fluids and Structures*, 1999, **13**, pp 551-578.
- BERTON, E., MARESCA, C. and FAVIER, D. A new experimental method for determining local airloads on rotor blades in forward flight, *Experiments in Fluids*, 2004, **37**, pp 455-457.
- FUJISAWA, N., TANAHASHI, S. and SRINAVAS, K. Evaluation of pressure field and fluid forces on a circular cylinder with and without rotational oscillation using velocity data from PIV measurement, *Measurement Sci & Tech*, 2005, **16**, pp 989-996.
- KURTULUS, D.F., SCARANO F. and DAVID L. Unsteady aerodynamic forces estimation on a square cylinder by TR-PIV, *Experiments in Fluids*, 2007, **42**, pp 185-196.
- VAN OUDHEUSDEN, B.W., SCARANO, F., ROOSENBOOM, E.W.M. CASIMIRI, E.W.F. and SOUVEREIN, L.J. Evaluation of integral forces and pressure fields from planar velocimetry data for incompressible and compressible flows, *Experiments in Fluids*, 2007, **43**, pp 153-162.